Textures and trace element chemistry of pyrite and chalcopyrite from Telfer Au-Cu deposit, W.A.: Implications for a multi-source ore system

Thesis submitted in accordance with the requirements of the University of Adelaide for an Honours Degree in Geology.

Anna Louise Ogilvie

November 2014

THE UNIVERSITY of ADELAIDE

TEXTURAL AND LA-ICP-MS TRACE ELEMENT CHEMISTRY ANALYSIS OF PYRITE AND CHALCOPYRITE FROM TELFER AU-CU DEPOSIT, W.A.

PYRITE AND CHALCOPYRITE ANALYSIS OF THE TELFER AU-CU DEPOSIT

ABSTRACT

The Telfer Au-Cu deposit, Paterson Province, W.A. is hosted within two doubly-plunging anticlines, the Main Dome and the West Dome. The deposit consists of vertically-stacked, stratabound Au-Cu mineralised horizons ('reefs') linked by associated stockwork, sheeted and discordant veins. The study targeted a better petrographic, mineralogical and geochemical understanding of pyrite and chalcopyrite in E-Reefs mineralization with the objective of placing additional constraints on ore genesis. Particular emphasis is placed on Type-4 pyrite as defined by Fargher (2012), notably the speciation of mineral inclusions within this type and their significance for a genetic model involving granitoid-sourced fluids. The trace element chemistry of the associated chalcopyrite was characterised by Laser-Ablation Inductively-Coupled Plasma Mass-Spectrometry (LA-ICP-MS) to identify whether a similar signature is present.

Back-scatter electron imaging established a number of mineral associations and inclusions within pyrite and chalcopyrite. These define a pronounced Sn-Bi-Ag geochemical signature in the E-Reefs. LA-ICP-MS data for pyrite, and particularly chalcopyrite, from the E-Reefs exhibit the same Sn-Ag-Bi geochemical signature, and are indicative of a granitophile character. Such a signature is unlike that of the Middle Vale Reef.

Arsenopyrite- and gersdorffite-bearing assemblages within crosscutting veins indicate a superposed hydrothermal event, in which additional elements, like As, were introduced to the system. There is also evidence of extensive ore remobilisation as the result of a later thermal event. These findings support a modified model of ore genesis for the Telfer deposit in which not all components in the ore fluid were leached from the surrounding sedimentary rocks but also involve fluids from adjacent granites. This has application not only to the Telfer deposit but carries implications for other ore systems in the Paterson Province. Results also contribute to ongoing work 'fingerprinting' chalcopyrite from different ore types to establish a basis for discriminating metal sources and fluid evolution.

KEYWORDS

Telfer, Au-Cu, Pyrite, Chalcopyrite, Textures, Laser-Ablation Inductively Coupled Plasma Mass-Spectrometry, Trace Element Chemistry

TABLE OF CONTENTS

LIST OF FIGURES AND TABLES

INTRODUCTION

The World-class Au-Cu Telfer deposit (1.8 Moz Au @ 0.79 g/t, 0.17 Mt Cu @ 0.23%; Newcrest Mining Limited 2014) is hosted within an exposed sequence of Paleo- to Neoproterozoic marine sediments surrounded by rocks of the Canning Basin, located to the west of the north-western Paterson Orogeny, Western Australia (Bagas 2004a). The orebodies are localised in two doubly-plunging anticlines called the Main Dome and the West Dome (Rowins *et al*. 1997). These dome structures consist of vertically-stacked, stratabound Au-Cu mineralised horizons ('reefs') linked by associated stockwork, sheeted- and discordant- veins. (Rowins *et al.* 1997).

Since discovery in 1972, a variety of models have been applied to explain the Neoproterozoic (~650 Ma) age 'Telfer-style' mineralisation. Earlier hypotheses included syngenetic exhalative (Tyrwhitt 1985), epigenetic replacement (Goellnicht *et al.* 1989) and the distal halo of a porphyry Cu-Au system (Dimo 1990). Rowins *et al.* (1997, 1998) considered that features of "Telfer-style" mineralization are attributable to a coincidence of several factors, with the current model taking into account the interrelationships between sedimentary environment, orogenesis and granite intrusions.

The granitoids are suggested to have assisted in driving large-scale thermal convection of heated saline waters sourced from the sedimentary host rocks and are not considered to be a major source of ore metals or sulphur at Telfer, Rowins *et al.* (1997).

A similar view has been endorsed in reviews of Australia's Proterozoic mineral systems (e.g. Pirajno & Bagas 2008). Constraints on the timing of ore formation are supported

by age data (e.g. Durocher *et al.* 2003), which infer that Telfer is likely a product of a mineralization event associated with the Miles Orogeny even if there remains uncertainty about the relative roles of orogenic thermal activity (ca. 680-630 Ma), post-orogenic magmatism (ca. 630-610 Ma) and possible overprinting during the Paterson Orogeny (ca. 550 Ma). This ambiguity led Groves *et al.* (2003) to consider the possibility that Telfer may actually belong to the intrusion-related category.

Fargher (2012) identified four discrete generations of pyrite at Telfer. Each generation of pyrite has a characteristic trace element and textural pattern. The four texture types are: (i) Early pyrite containing abundant gangue inclusions, chalcopyrite and carbonate. This generation commonly forms a distinctive core within larger pyrites; (ii) Euhedral As-, Co- and Ni-rich pyrite devoid of gangue inclusions (pervasive regional overprint?); (iii) Pyrite enriched in Co and Ni as oscillatory growth zones indicative of hydrothermal leaching of mafic rocks; and, (iv) Pyrite containing Sn, Bi, Cu ± Zn, Te and Au as inclusions (and possibly also in lattice-bound form) within As-Co-Ni-poor pyrite is potentially attributable to a second, granitic source.

Importantly, these texturally-defined sub-groups can also be defined chemically, albeit with some variation within each sub-set. However, interpretation is complicated since, in some case, individual pyrite grains record evidence of more than a single ‘texture’ or geochemical signature, as a result of sequential reworking. The pyrite textures and trace element signatures reported by Fargher (2012) support one of the following, or a combination thereof:

1. A single mineralising event where multiple sources of metal and/or sulphur is incorporated within the generation of pyrite; or alternatively,
2. A multi-stage ore genesis where the discrete pyrite characteristics reflect individual styles of mineralisation synchronous with geological events over time.
Subsequent deformation-induced grain-scale remobilisation of Au, Ag, Bi, Te, Cu, Sn, Co, Tl, Pb and As is common to all pyrite generations, explaining the heterogeneity observed within the trace element data.

Compared to previous studies, a greater geochemical complexity is evident in the data set; opening up the idea that not all components from the ore fluid were leached from the surrounding sedimentary rocks, but that the granitoids may have played a role as one of the sources for the metals in the deposit.

In this paper, we characterise aspects of mineralogy and petrography of pyrite from within sediments and reefs taken from diamond drill ore sourced from the West Dome deposit at Telfer. We aim to understand, in greater detail, whether Fargher's (2012) characterisation of pyrite texture types 2- and 3 is sustainable in the light of re-evaluation of the trace element data. The study also places emphasis on understanding the lesser studied Type-4 pyrite of Fargher and in particular the speciation of mineral inclusions within this type and its significance for a model involving granitoid-sourced fluids. In addition, the trace element chemistry of the associated chalcopyrite is characterised in order to identify whether a similar signature to the pyrite is present. This study therefore contributes to the debate concerning the style of mineralisation at the Telfer deposit by providing two additional datasets that provide additional evidence

in support of the hypothesis that "Telfer-style" mineralisation is attributable to a coincidence of several factors" (Rowins *et al.* 1997, 1998).

GEOLOGICAL SETTING

Regional Geology

The Paterson Orogeny is a Palaeoproterozic to Neoproterozoic region found in north-western Western Australia. The orogeny is a 2,000 km-long northwest trending belt of metamorphosed sedimentary and igneous rock (Williams & Myers 1990; Rowins *et al.* 1998; Langsford 2000). The Paterson orogeny, which hosts the Nifty Cu deposit and the Kintyre Uranium prospect, as well as the Telfer Au-Cu deposit, is located to the east of the Pilbra craton, adjacent to the Officer Basin and is overlain by the Canning Basin (Figure 1a) (Bagas 2004a; Fargher 2012).

The Paterson orogeny comprises of Palaeoproterozoic basement gneisses of the Rudall Complex, lying unconformably below the Neoproterozoic Yeneena Supergroup, followed by the covering Neoproterozoic Tarcunyah Group of the northwest Officer Basin (Langsford 2000; Bagas 2004a; Rowins *et al.* 1998).

The Yennena Supergroup is a >9 km-thick sequence of weakly metamorphosed marine sedimentary rocks (Williams & Myers 1990; Clarke 1991; Rowins *et al.* 1998) that hosts the Telfer Au-Cu deposit. The supergroup is subdivided into the Throssell Range and Lamil group (Bagas 2004a; Grey *et al.* 2005). The Lamil group conformably overlies the Throssell Range and comprises of the Isdell, Malu, Telfer, Puntapunta and Wilki Formations (Figure 1b).

The Malu and Telfer Formations are the host rocks for the mineralised reefs. The Malu Formation is thought to have been deposited in a high energy, prograding turbiditic environment (Fargher 2012). The 1500 m-thick series of massive to thickly bedded, metamorphosed, fine- to medium-grained quartzite and quartz sandstone with occasional thin interbeds of siltstone and mudstone supports this hypothesis (Newcrest 2014). The Malu Formation includes the rim-,median- and footwall-sandstones, the upper-, middle- and lower-Vale siltstones and the upper-, middle- and lower-Malu members (see Figure 1b). The mineralised veins within this formation include the Middle Vale Reef, M-, A-, B- and I30Q reefs (Figure 2), which are a series of stockwork, sheeted and discordant veins (Fargher 2012).

The Telfer Formation comprises an outer siltstone and camp sandstone members (Figure 1b) (Fargher 2012; Newcrest 2014). Consisting of a sequence of interbedded argillites and arenites, deposition is thought to have been in a shallow marine environment (Newcrest 2014). The mineralised E-Reefs are found within the outer siltstone member (Figure 1b).

The first of three tectonic events defining the Paterson Orogeny, is the SW and W-directed thrust stacking and complex folding of the Rundall Group during the Yapungky Orogeny (ca. 1830-1765 Ma) (Geological Survey of Western Australia 1996, Maxlow & Wilson 2005). This is interpreted to be the product of convergence between the North and Western Australian cratons (Bagas 2004b; Maxlow & Wilson 2005; Pirajno & Bagas 2008).

The Miles Orogeny (ca. 680-630 Ma) involves two regional-scale compressive stress regimes differentiated by a progressive 15° anti-clockwise rotation (Bagas 2004b; Maxlow & Wilson 2005). This led to the evolution of the Main and West domes as a result of bedding dilation and quartz-pyrite reef mineralisation (Maxlow & Wilson 2005; Maxlow 2007).

Lastly, the Paterson Orogenic event (ca. 550 Ma) saw progressive clockwise rotation of principle compressive stresses (Bagas 2004b). The emplacement of this event allowed the occurrence of multiple phases of granite intrusions, associated contact metamorphism, reactivation of and development of mineralisation (Bagas 2004b). The final post orogenic event was the extensional regimes in the Officer and Canning Basins resulting in the intra-cratonic basin infill of arenaceous strata (Maxlow 2007).

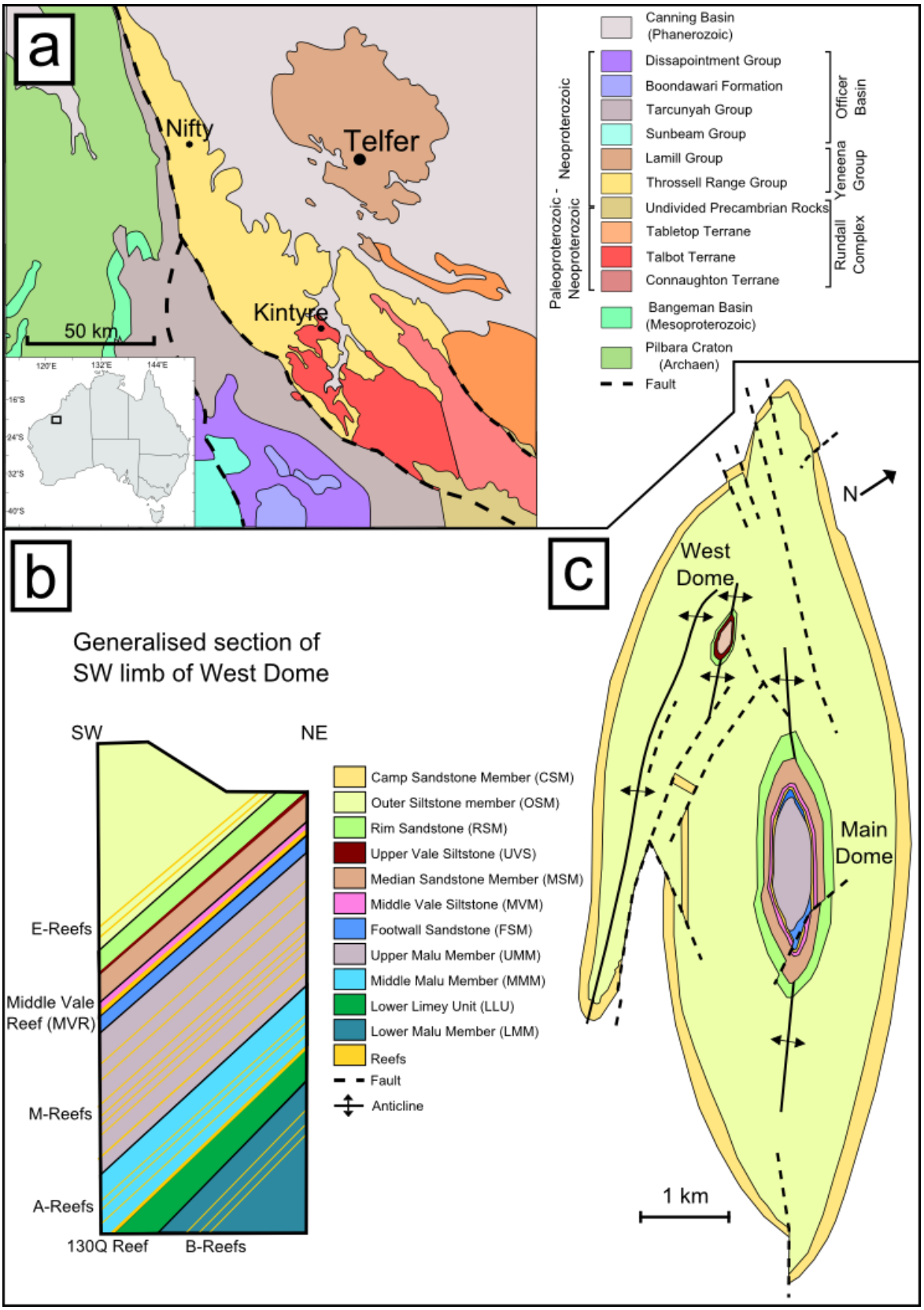

Figure 1 (A) Geological Map of the Paterson province and locations of the Telfer Au-Cu and Nifty Cu deposits and the Kintyre U prospect, Map modified from Fargher (2012) after Bagas (2004a). (B) A schematic generalised section of the SW limb of the West Dome deposits looking WNW adapted from Fargher (2012). (C)Telfer mine geology and locations of the West- and Main-Dome, adapted from Goellnicht et al. 1989.

Telfer Mine Geology

The Telfer Au-Cu deposit is localised in two doubly-plunging, asymmetric anticlines called the Main Dome and the West Dome (Figure 1c) (Rowins *et al.* 1998; Newcrest 2014). These dome structures consist of vertically-stacked, stratabound Au-Cu mineralised horizons ('reefs') linked by associated stockwork, sheeted, and discordant veins (Rowins *et al.* 1997). Primary mineralisation was overprinted by surface weathering processes (Newcrest 2014). In many cases the reefs cannot be correlated between the two domes because the deeper reefs have not always undergone intensive supergene Au enrichment (Rowins *et al*. 1997, 1998). The West dome fold structures have shallow to moderately dipping western limbs and moderate- to steep-dipping eastern limbs, forming a topographical high in the Northwest region of the mine (Newcrest 2014).

The current model for 'Telfer style' mineralisation considers a coincidence of several factors, taking into account the interrelationships between sedimentary environment, orogenesis and granite intrusions (Rowins *et al.* 1997). Although the granitoids are not considered a major source of ore metals or sulphur at Telfer, Rowins *et al.* (1997) suggested they were instrumental in driving large-scale thermal convection of heated saline waters sourced from the sedimentary host rocks. This was assisted by the presence of deep basement faults and permeable host rocks that permitted extensive transport of ore fluids, and abundant chemical traps in the host sequence. However, the uncertainty about the relative roles of orogenic thermal activity (ca. 680-630 Ma), post-orogenic magmatism (ca. 630-610 Ma) and possible overprinting during the Paterson

Orogeny (ca. 550 Ma), led Groves *et al.* (2003) to consider the possibility that Telfer may actually belong to the intrusion-related category.

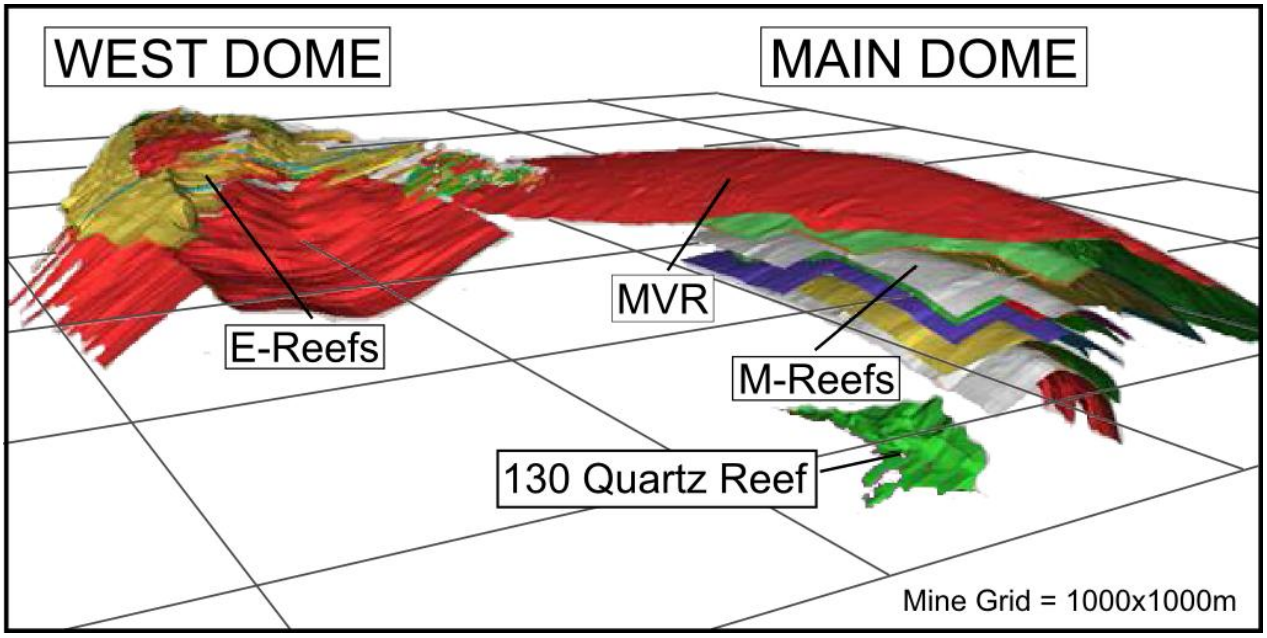

Figure 2 Oblique Schematic View of the Telfer Au-Cu Deposit looking north, showing divisions of the deposit in the Main- and West-Dome (Redrawn from Newcrest Mining 2014). The figure also shows the key mineralised zones of the E-Reefs, Middle Vale Reefs (MVR) and M-Reefs.

Trace Element Chemistry of Pyrite and Chalcopyrite

Many studies on trace element distributions in economically significant metal sulphides have been conducted over the past 30 years. The main issues with trace element studies are determining when certain trace elements are specific to individual minerals and whether a trace element is homogenously distributed within the crystal lattice (solid solution), or is present as a sub-microscopic inclusion of a discrete mineral.

Pyrite is the most studied with respect to trace element content. Elements that are typically included as extensive solid solutions into the pyrite lattice comprise of As, Co and Ni (e.g. Kouzmanov *et al.* 2002). Marked zonation patters, expressed by heterogeneous concentrations of these elements can provide a record of ore fluid

evolution. The preservation of textures and distinct trace element distribution patters are often important evidence for multi-stage genetic development of an ore deposit (Arehart *et al.* 1993; Fleet *et al.* 1993; Oberthür *et al.* 1997; Genkin *et al.* 1998; Kouzmanov *et al.* 2002). Different pyrite generations recognized within pyrite can assist in the identification of sequential stages of mineral growth within multiphase or overprinted mineral systems (Large *et al.* 2007, 2009; Cook *et al.* 2009; Sung *et al.* 2009; Thomas *et al.* 2011; Winderbaum *et al*. 2012).

Sulphide minerals, in particular pyrite and arsenopyrite can also host for gold (Harris 1990). In some sulphide bearing refractory ores, 'Invisible gold' can contribute the majority of the gold found in the deposit (Cook & Chryssoulis 1990.). 'Invisible gold' includes sub microscopic inclusions, gold as a solid solution or the chemically bound gold found within the sulphides in some gold ores (Harris 1990).

Compared to other common sulphides, there has been relatively little study of the ability of chalcopyrite to incorporate trace elements. As with other sulphides, an understanding of chalcopyrite trace element chemistry is significant for establishing the behaviour of valuable elements that could potentially be extracted economically and also for the issue of sulphide breakdown in waste dumps, potentially leading to release of toxic elements (Cook *et al*. 2013). Chalcopyrite has been demonstrated to be an excellent host for silver in solid solution (Harris *et al*. 1984; Cabri *et al.* 1985) but is generally a poor host for gold (Cook & Chryssoulis 1990). Other studies (e.g. Huston *et al.* 1995; Moggi-Cecchi *et al.* 2002) have report other examples of trace element substitutions between Co, Ni, Mn, Zn and Sn for Cu and/or Fe; and Se, Fe and As for S have been proposed

by Taseska *et al.* (2008). A first reconnaissance study of the distribution of 28 trace elements in 44 ore samples of wide-ranging genesis has been undertaken by Crowe (2014).

Grain scale compositional zoning of trace elements in other common sulphides such as sphalerite or galena is often a valuable source for information about the ore genesis (e.g. Cook *et al.* 2009; George *et al.* 2014). This is, however, dependent on a sound understanding of the concentrations and substitution mechanisms of minor/trace elements in the sulphides. No intra-grain zoning is reported for chalcopyrite and it is doubtful that this mineral displays primary zoning. The few indications of grain-scale heterogeneity are likely reflective of (secondary) sub-solidus diffusion (N. Cook pers. comm. 2014).

METHODS

Analytical Approach

Combining individual techniques such as scanning electron microscopy (SEM), electron probe microanalysis (EPMA) and laser ablation inductively-coupled plasma mass spectrometry (LA-ICP-MS), allows the extraction of information on both the grain-scale spatial and chemical distributions of elements within minerals (e.g. Fryer *et al.* 1995). The LA-ICP-MS technique offers quantification of trace element concentrations, especially for those where extremely low limits of detection are required coupled with reasonable spatial resolution (Fryer *et al*. 1995).

Sampling

Sampling targeted suitable drill core with significant representative intersections containing pyrite and chalcopyrite from the West Dome deposit. Mineralised reef and syngenetic pyrite intersects were identified from assay results, Newcrest log cores were sampled. The aim was to have a sample suite that was spatially representative of the E-reefs of the West Dome.

Experimental Details

Scanning electron microscopy (SEM) was conducted on samples to give a clear identification of the minerals of interest and their relationships. The SEM work involved the use of a Quanta 450 instrument, equipped with an EDAX team energy dispersive X-ray spectroscopy (EDS) silicon drift detector (SDD) and back-scatter electron (BSE) detector, to produce digital images of the samples. BSE imaging allows information about the mineral textures, mineral inclusions and compositional zoning to can be observed and visually captured. A Cameca SX-51 Instrument was used to obtain quantitative major and minor element compositional data for minerals whose composition can vary. LA-ICP-MS was used to find the quantitative trace element concentrations. A Resonetics M-50-LR 193-nm Excimer laser microprobe coupled to an Agilent HP-7700cx Quadrupole ICP-MS was used for analysis.

Full details of the analytical methodology used for the LA-ICP-MS spot analysis and element mapping, including standardisation and calibration routines, are given in Appendix A.

OBSERVATIONS AND RESULTS

Mineralogy and Textures

The E-Reefs consists of laminated argillaceous, calcareous and minor carbonaceous siltstone and inter-bedded sandstones. Pyrite and chalcopyrite are the most common sulphides. Pyrite is observed as varying combinations of euhedral, massive anhedral, milled and brecciated grains. Grain size was generally coarse (1 mm to >1 cm). The euhedral pyrite grains are generally smaller in size and almost always found as single disseminated grains within the siltstone. Larger, massive, milled and brecciated pyrite grains were usually seen as vein filling with quartz and, less commonly, carbonates. Fractures were often observed in the clusters pyrite of the veins; however the singular, euhedral grains were found to be less fractured or show no fracturing. Chalcopyrite grains are observed as either massive grains in the quartz-carbonate veins or as inclusions within pyrite. Other minerals occurring as inclusions (<2 mm) in the pyrite and as vein fill include quartz, carbonates and muscovite.

Sample 49, on the other hand is used as a comparison and was sourced from the Middle Vale Reef. This consists of thinly bedded, fine grained argillaceous siltstone and claystone with minor inter-bedded carbonaceous limestone and calcareous sandstone. The gangue mineralogy of the sulphide-bearing rock includes quartz, carbonates and potassium feldspar.

A number of mineral associations and inclusions defining the pronounced Sn-Bi-Ag geochemical signature in the E-Reefs were seen within both pyrite and chalcopyrite. The identity of these minerals was confirmed by SEM-EDAX.

Although chalcopyrite is the dominant Cu-bearing mineral, a range of other Cu-(Fe) sulphides (bornite, chalcocite, covellite and cubanite) were observed, often in the same regions of the sample (Figure 3a). Two generations (?) of chalcopyrite were noted, with one of the textures being a more inclusion rich massive grains and the other having a 'cleaner' (Inclusion-free) appearance, which is seen to infill fractures (Figure 3b). The occurrence of cubanite ($CuFe_2S_3$) as exsolution lamellae within chalcopyrite is a good indicator of a high temperature hydrothermal environment (Figure 3c).

Covellite (CuS) was observed forming an outer rim around chalcopyrite that had been replaced by bornite (Figure 3d). Overprinting of chalcopyrite by bornite (Figure 3e) is also suggested by the inclusions of chalcopyrite and the 'criss-crossing' texture of the bornite grains, possibly indicating exsolution within that bornite at a scale too small to be readily resolved. Fractures in chalcopyrite were often filled by secondary sulphide minerals, such as anilite (Cu_7S_4) at the boundary of quartz veins that crosscut the massive chalcopyrite. The texture of anilite suggests its formation resulted from the interaction of later hydrothermal or supergene fluids with chalcopyrite (Figure 3f). Chalcocite can also be observed and displays similar textures to the anilite (Figure 4a). The secondary nature and textures of these minerals are indicators of multistage genesis, even if their absolute timing cannot be resolved. A further Cu-sulphide, geerite (Cu_8S_5) is observed at the boundary between chalcopyrite and kesterite with a void in massive pyrite (Figure 4b). Geerite is usually observed to replace sphalerite, indicating this occurrence is a result of secondary mineralization.

Sphalerite was commonly observed as vein filling within pyrite and chalcopyrite. Minor amounts of sphalerite were noted as inclusions within pyrite (Figure 4c), or as angular grains in quartz voids (Figure 4d). Sphalerite was also observed with quartz, filling fractures in the ~brecciated pyrite (Figure 4e).

Cassiterite (SnO_2), këserite ($Cu_2(Zn,Fe)SnS_4$) and stannite ($Cu_2(Fe,Zn)SnS_4$) were observed in every sample, almost exclusively as inclusions (commonly composite) within chalcopyrite, and frequently associated with voids (or pores?) in the host sulphide (Figures 4b,f and 5a). The sizes of these Sn-mineral inclusions ranged from 10-50 µm of and they are typically rounded to sub-angular in shape. Smaller inclusions of mostly stannite (<5 µm) were also identified within pyrite. These grains displayed no obvious orientation, occur as clusters and appear to represent products of exsolution during pyrite cooling.

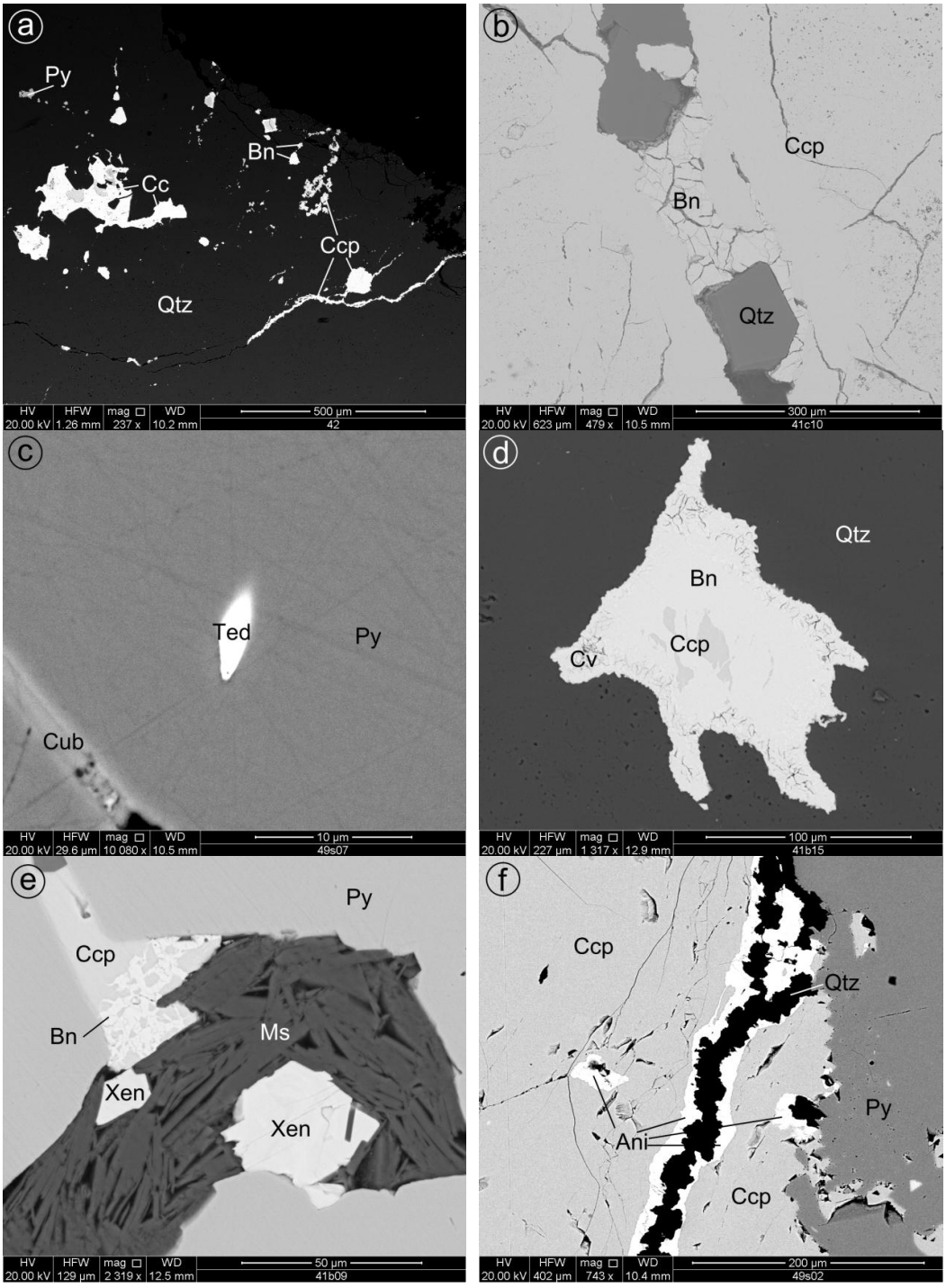

Figure 3 Back-scatter electron images of various Cu-Bi-P mineralogy. (a) Coexisting bornite (Bn),chalcocite (Cc) and later (?) fracture-filling chalcopyrite (Ccp) within quartz (Qtz). (b) Fractured massive chalcopyrite grain, filled with bornite and quartz. The chalcopyrite appears to have two textures, a more porous (?) form makes up a large percentage of the grain, while a smooth, clear looking chalcopyrite texture lines the edges of the fracture. (c) Tetradymite (Ted) grain with nearby cubanite (Cub) vein in pyrite. (d) Fractured covellite (Cv) rim surrounding a chalcopyrite grain that is overprinted by later (?) bornite, in quartz. (e) Muscovite (Ms) filled vein with xentotime inclusions, within Massive pyrite. Bornite overprints chalcopyrite in a second vein within the pyrite. (f) Mutual boundary of pyrite and chalcopyrite. Fracture filling by anilite (Ani) coats the edges of the fracture, with quartz filling the centre. Two larger anilite grains fill voids within the chalcopyrite grain.

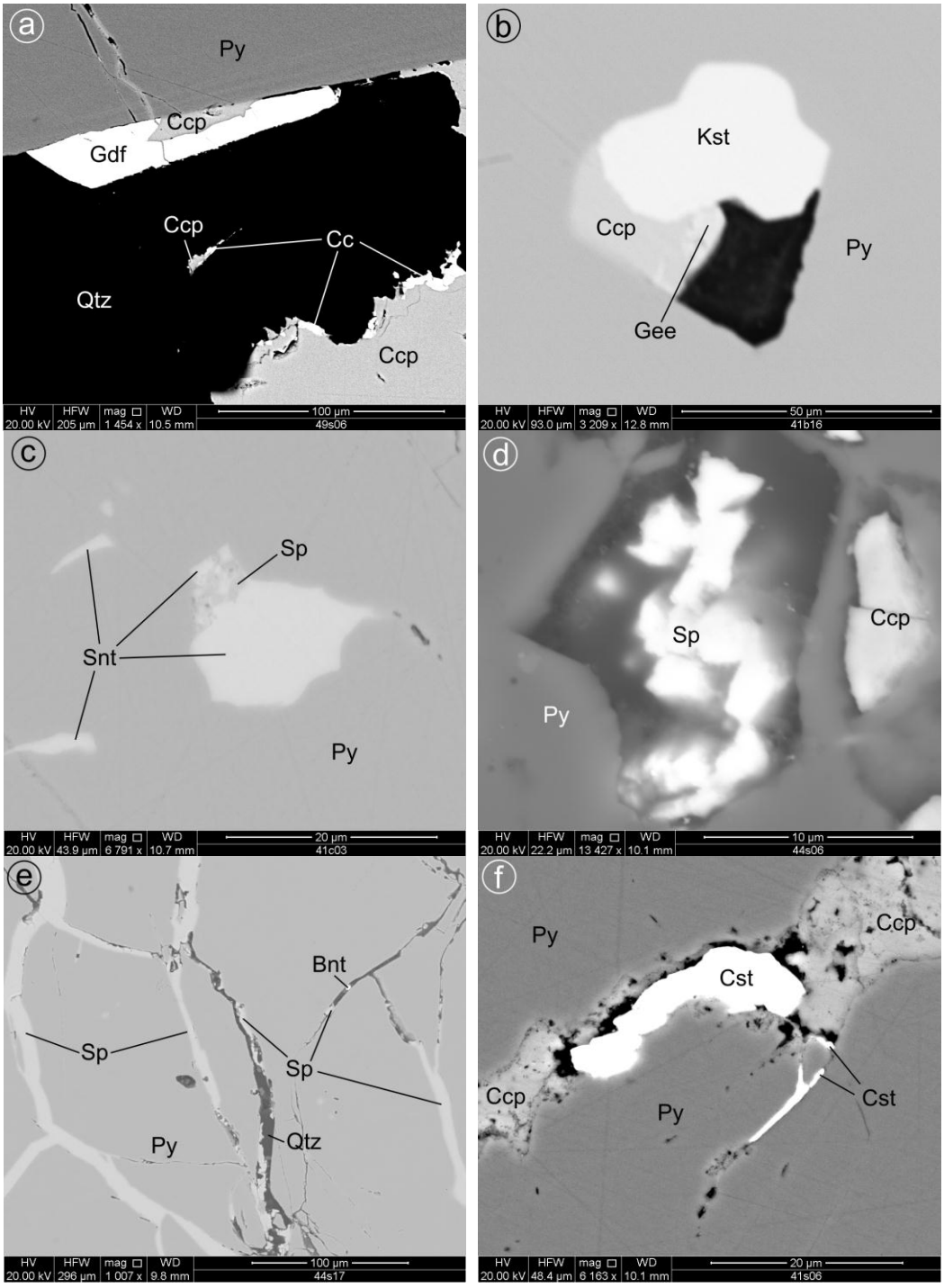

Figure 4 Back-scattered images of Cu-Sn-Zn mineralogy. (a) Quartz filling between the edges of pyrite and chalcopyrite grains. A thin rim of chalcocite (Cc) lines the edges of the massive and smaller central chalcopyrite grains. At the edge of the pyrite grain sits a chalcopyrite grain surrounded by gersdorffite (Gdf). (b) Grains of këstérite (Kst), chalcopyrite and geerite (Gee) fill a void in massive pyrite. (c) Massive pyrite grain with inclusions of sphalerite over printed by later (?) stannite (Snt) grains. (d) Angular sphalerite (Sp) and chalcopyrite grains within massive pyrite voids. (e) Massive pyrite with sphalerite and quartz (Qtz) filled veins, with a small grain of bastnäsite-(Ce) (Bnt). (f) Massive pyrite (Py) grain with chalcopyrite (Ccp) and cassiterite (Cst) filled veins.

Both arsenopyrite (FeAsS) (Figure 5b) and gersdorffite (NiAsS) (Figure 4a) are observed. These minerals are restricted to the selvages of quartz microveins that crosscut pyrite. The cross-cutting nature on the veins and the 'boundary-hugging' tendency exhibited by both minerals indicates they were generated a hydrothermal event, possibly an overprinting event in which additional elements, like As, were introduced to the system.

Hematite grains, ~5 µm in size, are observed in quartz veins within massive pyrite (Figure 5c). The angular nature of the hematite and the lining of chalcopyrite at the boundary of the quartz vein also indicates formation during a secondary event, presumably at different fS2-fO2 conditions. Replacement of pyrite with chalcopyrite is evident within some hematite veins. Bismuth minerals are represented by bismuthinite, Bi_2S_3 (Figure 5d), and tetradymite, Bi_2Te_2S (Figure 3c). Both minerals are observed as inclusions in pyrite and vary from 2-5µm in size.

Grains of electrum were observed in 7 of the 12 samples, and range in size from 5-20 µm. Native gold grains were seen at <5 µm in size, however these are relatively rare. Gold minerals typically occur either within fractures and voids in pyrite (Figures 5e-f), as inclusions in chalcopyrite (Figure 6a), in quartz between sulphide minerals (Figure 6b), and in pyrite veins infilled by what is interpreted as secondary chalcopyrite (Figure 6c-d). Remobilisation of minerals and their component elements within the samples is shown through a grain of electrum sitting within a crosscutting secondary (?) chalcopyrite vein (Figure 6d). This clearly suggests mobilization as the result of a post-formational thermal event.

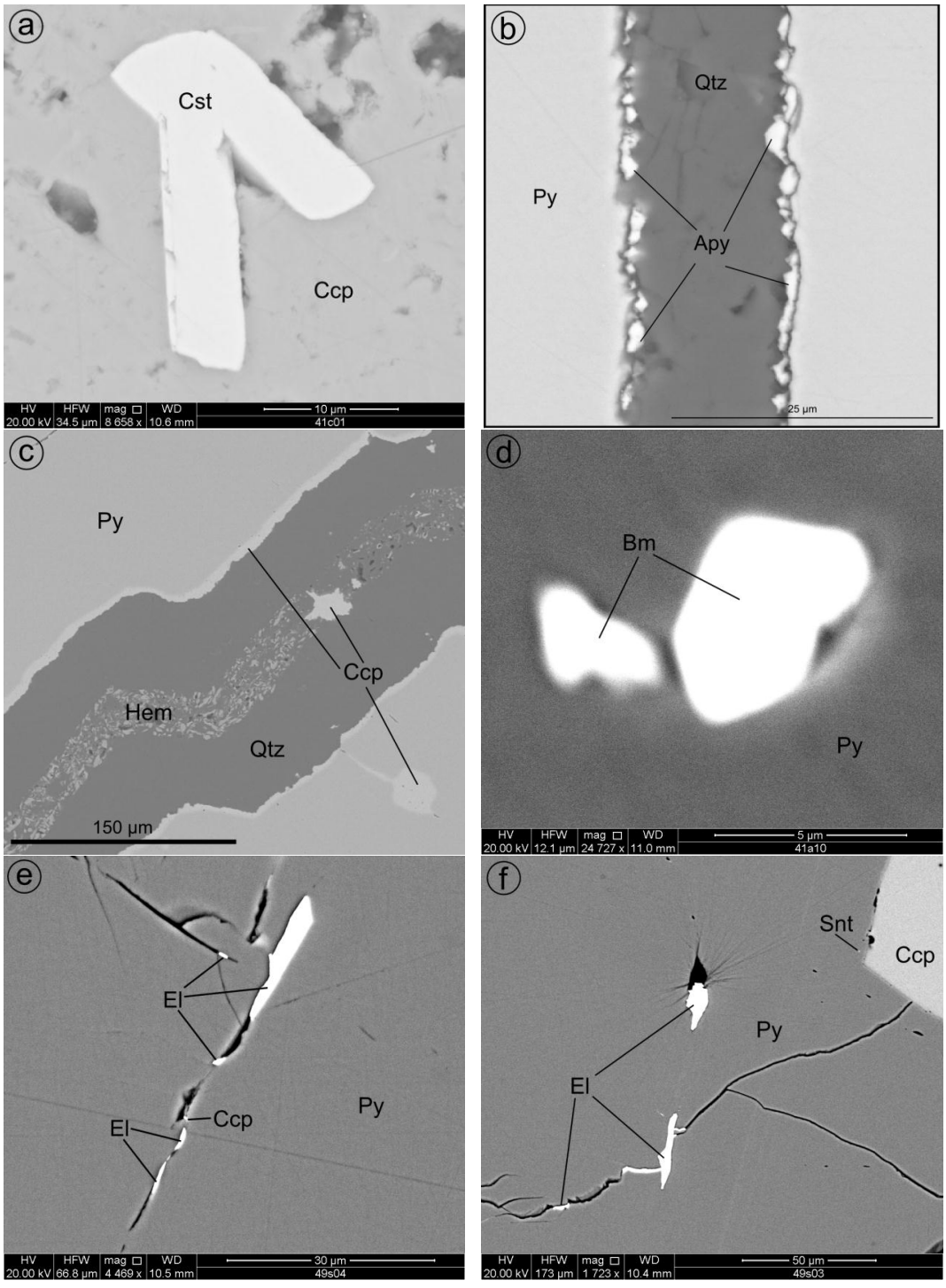

Figure 5 Back-scattered image of As-Ag-Fe-Sn-Au-Bi mineralogy. (a) Cassiterite grains sit within massive chalcopyrite voids. (b) Arsenopyrite (Apy) lining the edge of a quartz (Qtz) vein in massive pyrite (Py). (c) Fracture filled with hematite (Hem), quartz and chalcopyrite in massive pyrite. (d) Bismuthinite (Bm) grains in massive pyrite. (e) Grains of electrum (El) within fractures in massive pyrite (py). (f) Grains of electrum within fractures and a void in pyrite. A small grain of stannite (Snt) occurs at the mutual boundary of pyrite and chalcopyrite.

Native silver was observed at the grain boundary between pyrite and quartz (Figure 6e). Native silver varies in size from <2-20 µm, with some grains appearing to be exsolved from the neighbouring pyrite grain.

Representative SEM-EDS analyses of minerals cassiterite, këwhile sterite, stannite, tetradymite and electrum are presented in Table 3. Of particular note is the extensive compositional variation expressed by minerals of the stannite group.

The Y-REE-phosphate xenotime is a common inclusion in both quartz and pyrite. The mineral, occurring as blastic, compositionally zoned grains, is often seen filling voids in pyrite and as inclusions in quartz near pyrite and chalcopyrite grain margins (Figures 3e and 6f). A grain of bastnäsite-(Ce) [(Ce,La)(CO_3)F] was also observed within a sphalerite filled vein in massive pyrite (Figure 4e)

Gangue minerals quartz, muscovite (Figure 3e) and potassium feldspar are observed as the fracture- and vein-fillers, crosscutting and surrounding the sulphides.

Table 1 SEM-EDS analysis of Sn-, Bi-, and Au-bearing minerals.

						Wt%				
O	19.04	18.3								
S						27.94	26.93	30.04	30.1	3.97
Cl	0.21									
Fe		1.73	2.23				6.07	5.66	5.26	3.37
Co		1.5	1.08							
Cu						31.44	27.8	34.49	34.28	
Zn						14.83	12.1			
Mo	1.1									
Ag			12.78	16.6	40.74					
Sn	79.65	78.47				25.79	27.1	29.81	30.36	
Te										33.61
W			2.17							
Au			81.74	83.4	59.26					
Bi										59.05
Totals	100.00	100.00	100.00	100.00	100.00	100.00	100.00	100.00	100.00	100.00
Formula	SnO_2			(AuAg)		$Cu_2(Zn,Fe)SnS_4$		$Cu_2(Fe,Zn)SnS_4$		Bi_2Te_2S
Mineral	cassiterite			electrum		Kësterite		stannite		tetradymite

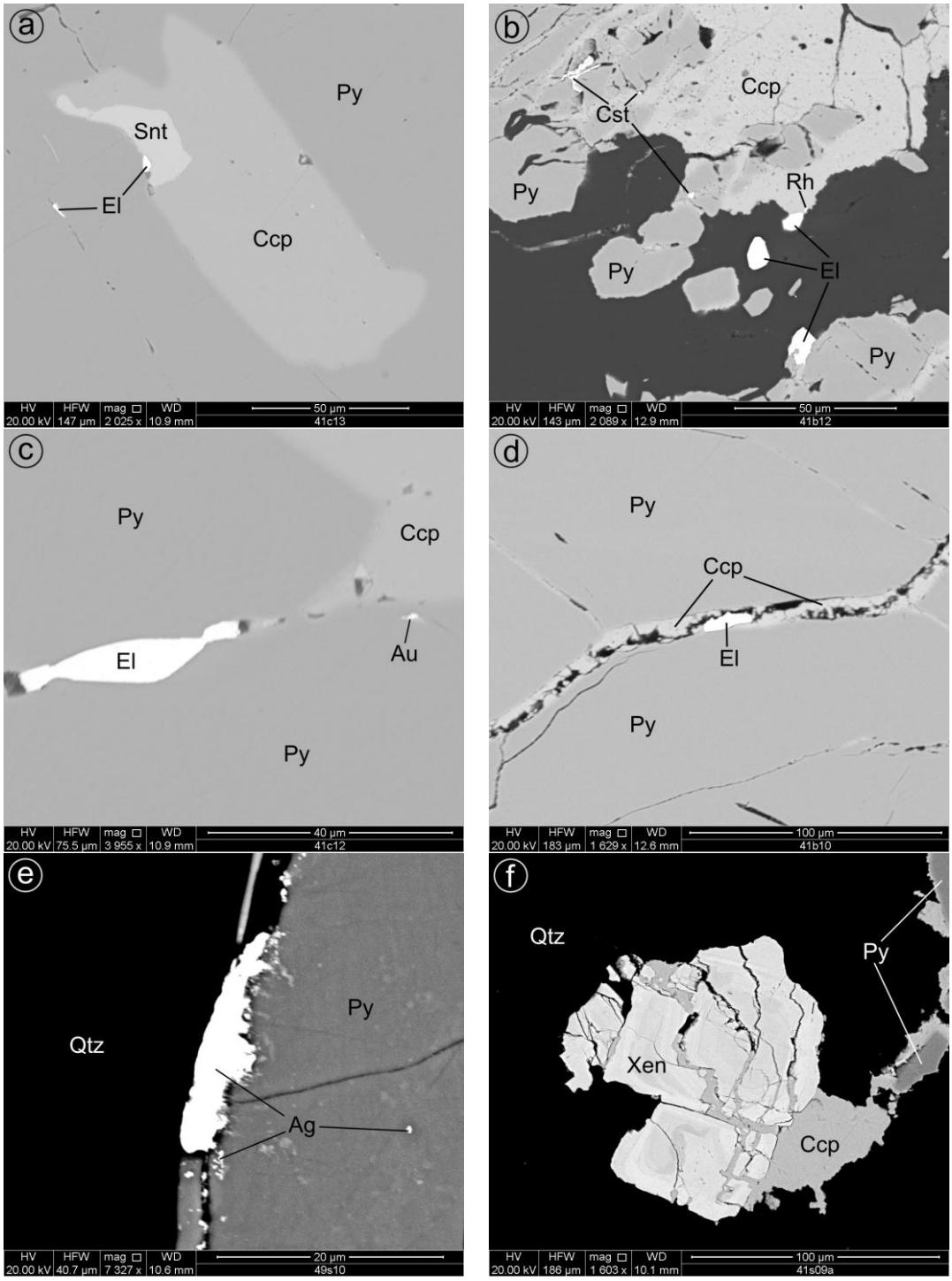

Figure 6 Back-scatter electron images of Au-Ag-P-Sn minerals. (a) Coarse pyrite with inclusions of pyrite, stannite (Snt) and electrum. (b) Clustered pyrite grains with surrounding chalcopyrite and quartz (Qtz). Three electrum grains occur in quartz at chalcopyrite-pyrite boundaries. Cassiterite (Cst) inclusions are present within pyrite. (c) Electrum within a chalcopyrite-bearing vein in massive pyrite. A grain of native gold (Au) is observed at the boundary of the vein and pyrite. (d) Grain of electrum within chalcopyrite vein crosscutting massive pyrite. (e) Silver (Ag) grains at the edge of a pyrite grain surrounded by quartz. (f) Highly fractured xenotime (Xen) filled with chalcopyrite in quartz at the edge of a massive pyrite grain.

LA-ICP-MS Analysis

LA-ICP-MS trace element analysis was conducted on 7 samples to identify the trace element chemistry of the pyrite and chalcopyrite. Tables 2 and 3 summarize the minor and trace element concentrations in 73 and 72 spot analyses of pyrite and chalcopyrite, respectively.

Pyrite trace element chemistry data for cobalt, copper and arsenic (Table 2) showed values spanning more than five orders of magnitude (Co: 0.45 to 2,612 ppm, Cu: 0.30 to 45,027 ppm and As: 0.42 to 10,341 ppm). All three elements have average standard deviations that exceed their average concentrations. The highest overall Cu values were seen in sample 41a, whereas sample 41c produced the lowest values for Cu.
Nickel concentrations spanned within two orders of magnitude, nevertheless the concentration values were consistently high (e.g. 18 to 2,993 ppm).

A varied range of concentrations were obtained for Pb and Bi, as individual spot analyses ranged over four orders of magnitude. Their average standard deviations are both higher than the average mean concentrations of the elements.

Relatively low values for Ag, Sn and Te were observed, except for two Sn values (800 and 1,134 ppm) which were contrary from the norm. It is thought that these higher concentration results are due to laser ablating inclusions lying at sub-surface within the host pyrite grain.

Pyrite from the Middle Vale Reef in sample gave similar results to the samples from the E-Reefs. For all pyrite samples, the average standard deviation seems to be higher than the average mean, except for V, Ni and As, which had average standard deviations below the average mean. Indium, Hg and Tl mostly showed concentration values lower than the respective minimum detection limits; the proportion of values that exceeded the detection limits are shown at the bottom of Table 2.

Trace element analyses of chalcopyrite (Table 3) showed the presence of a greater number of elements at measurable concentrations within the chalcopyrite.
In contrast, chalcopyrite from sample 49 shows generally low trace element concentration values.

The following results are discussing the E-Reefs values only.
Cobalt concentrations varied by 4 orders of magnitude (e.g. 1.4 – 20,940 ppm). The concentrations of Ni also showed extreme variation (up by 3 orders of magnitude, e.g. from 1 to 2,184 ppm). All standard deviations for Co and Ni were higher than their mean value, also indicating the large variation of these element concentration values in the host chalcopyrite. Such variation may indicate the presence of grain-scale compositional zoning, which has not been reported in chalcopyrite up until now.
Consistent zinc concentrations are noted for E-Reefs chalcopyrite; however sample 49 shows higher concentrations of zinc than the E-Reefs samples.

Lead concentrations in E-Reefs chalcopyrite are generally in the hundreds of ppm. The highest measured Pb concentration is 567 ppm. For sample 49, the Pb values are much

lower, ranging from 0.29-1.9 ppm. Concentration values for Ag and Au show a similar trend to those of Pb; their concentrations in E-Reefs chalcopyrite are generally higher than in sample 49 (E-reefs Ag: 14-132 ppm, Au: 1.3-8.1 ppm; Sample 49 Ag: 0.48-8.2 ppm, Au: 0.15-0.16 ppm).

Tin displays consistent concentration values in chalcopyrite, typically in the hundreds of ppm range, excluding one lower concentration value each from samples 42 (11 ppm) and 43 (0.89 ppm). Indium concentrations in E-Reefs chalcopyrite certainly vary compared to sample 49 which has very constant values (~13-14 ppm).Bismuth values vary between samples. There does not however seem to be a specific change in values when compared to sample 49.

The observed trace element concentration data for chalcopyrite from the E-Reefs clearly show that the same elements identified as inclusions are also present in the sulphide lattice at significant levels, and that these patterns are distinct from those in sample 49. These two important observations may be evidence either of a different event forming the E-Reefs, or a distinct source, or that physical-chemical conditions of sulphide precipitation differed (e.g. higher temperatures) to enable greater quantities of certain elements to enter the chalcopyrite structure. These themes are taken up in the 'Discussion' section below.

Table 2 Summary of minor and trace element concentration data for pyrite (ppm).

		Na	V	Co	Ni	Cu	As	Ag	Sn	Sb	Te	Ba	Au	Pb	Bi
41a	**Mean**	46.4	0.14	457	624	1287	3624	0.25	3.1	0.57	2.4	4.8	0.10	7.7	14
	S.D.	54.1	0.07	674	344	1855	3173	0.13	3.8	0.77	2.1	4.1	0.07	7.4	15
	Max	168.5	0.25	2120	1010	5541	10341	0.48	10.4	2.6	7.8	13	0.21	24	51
	Min	4.0	0.14	16	59	1.3	313	0.04	0.23	0.10	0.41	0.90	0.04	0.06	0.02
41b	**Mean**	7.6	0.10	261	922	405	569	0.12	146	0.11	1.2	1.7	0.03	2.2	2.9
	S.D.		0.04	253	603	489	1025	0.16	340	0.11	1.1			4.2	3.4
	Max	26	0.19	715	2063	1297	3470	0.54	1134	0.31	3.3	7.3	0.14	12	11
	Min	4.0	0.13	0.45	259	0.61	0.42	0.02	0.05	0.08	0.32	1.0	0.03	0.04	0.02
41c	**Mean**	3.6	0.14	653	909	21	81	0.05	7	0.10	1.5	0.64	0.11	0.14	4.1
	S.D.	4	0.07	864	715	32	143	0.06	21	0.12	2.9	0.4	0.26	0.13	11
	Max	15	0.27	2612	1990	81	474	0.21	67	0.43	9.7	1.9	0.84	0.38	35
	Min	4.2	0.19	16	189	1.4	1.1	0.06	0.32	0.12	0.54	1.0	0.06	0.05	0.03
41s	**Mean**	22	0.17	133	743	4197	124	0.82	101	0.35	5.4	6.6	0.18	6.5	14
	S.D.	28	0.07	129	450	13545	222	2.3	245	0.70	7.6	9.1	0.35	12	17
	Max	78	0.28	454	1607	45027	742	7.9	800	2.4	22	28	1.2	42	52
	Min	4.6	0.16	22	203	1.2	0.99	0.05	0.28	0.10	0.49	1.7	0.04	0.04	0.03
42	**Mean**	10	0.24	513	1064	886	1707	0.20	3.3	0.22	2.4	2.5	0.20	1.4	11
	S.D.	18	0.37	443	988	1989	1864	0.23	6.0	0.21	2.7	3.9	0.36	1.8	10
	Max	59	1.3	1225	2993	6318	5402	0.61	20	0.72	9.3	11	1.2	5.3	25
	Min	2.5	0.12	2.1	28	1.5	34	0.03	0.21	0.10	0.31	0.9	0.03	0.06	0.02
43	**Mean**	7.3	0.17	371	734	2330	1825	0.17	0.9	0.16	1.7	0.93	0.08	0.56	3.2
	S.D.	13	0.03	547	599	7332	1280	0.44	2.4	0.26	3.7	0.83	0.217	0.58	4.5
	Max	41	0.23	1842	1860	23198	3337	1.4	7.6	0.87	12	3.0	0.7	1.8	12
	Min	2.7	0.14	12	27	0.30	180	0.03	0.21	0.12	0.29	0.98	0.03	0.05	0.02
49	**Mean**	4.9	0.23	788	526	38	2278	0.76	0.14	0.14	1.3	0.70	0.04	0.98	5.9
	S.D.	6	0.08	1892	463	103	1234	1.4	0.06	0.13	1.9	0.55	0.028	1.4	9.5
	Max	18	0.35	6135	1465	330	4879	4.6	0.32	0.40	5.2	2.3	0.09	4.2	27
	Min	3.5	0.14	2.0	18	1.9	58	0.00	0.24	0.11	0.42	1.1	0.04	0.04	0.02

Notes
In: Only two samples showed any detectable concentrations: 41a mean 0.04, S.D. 1.1, max 3.4 and min 0.01, and sample 41b mean 0.64, S.D. 1.4, max 4.7 and min 0.01ppm.
Hg: Two samples showed data, 41a mean 0.08, S.D. 0.04, max 0.15 and min 0.10ppm, and sample 43 mean 0.06, S.D. 0.02, max 0.09 and min 0.05ppm.
Tl: Two samples showed any data, sample 41a mean 0.04, S.D. 0.06, max 0.20 and min 0.01 ppm and sample 42 mean 0.23, S.D. 0.38, max 1.2 and min 0.01 ppm.

Table 3 Summary of minor and trace element concentration data for chalcopyrite (ppm).

	Na	Co	Ni	Zn	Ga	As	Mo	Ag	Cd	In	Sn	Sb	Au	Hg	Tl	Pb	Bi
41a Mean	135	852	64	99	0.95	245	1.9	30	1.0	6.4	632	9.2	2.8	0.61	157	209	24
S.D.	72	1171	96	274	0.67	395	4.2	33	0.59	2.3	155	9.5	2.0	0.24	210	139	21
Max	287	4076	331	879	1.8	1352	14	109	2.4	11.5	933	34	6.6	0.86	573	495	63
Min	31	4.0	1.4	9.0	0.46	2.3	0.76	1.8	1.1	3.9	428	0.60	0.15	0.42	0.07	86	1.1
41b Mean	1149	195	19	354	2.65	77	0.8	6	2.9	17	790	3.6	0.79	0.24	30	111	5.9
S.D.	1723	333	26	768	1.57	201	1.2	11	3.3	6.2	124	3.6	1.5	0.08	69	179	8.1
Max	4703	863	70	2528	6.3	648	4	34	9.6	25	989	12	4.8	0.40	223	567	26
Min	19	4	1.5	12.0	0.48	1.8	0.79	0.18	1.1	5.3	585	0.70	0.14	0.41	0.13	5.4	1.2
41c Mean	226	3286	285	58	1.3	927	5.4	89	3.1	20	831	14	4.8	0.73	625	180	2.9
S.D.	243	5463	542	76	1.5	844	5.4	38	1.2	3.8	291	6.4	2.2	0.29	220	69	1.9
Max	904	15981	1765	284	4.1	2454	16	132	5.1	25	1565	23	7.5	1.2	802	268	5.7
Min	51	15.7	1.5	14.09	0.51	2.1	0.87	0.55	1.4	12	490	1.3	0.17	0.46	0.97	33	0.34
41s Mean	287	516	34	132	1.3	354	1.8	49	1.6	18	874	9	2.5	0.54	288	121	2.7
S.D.	396	1197	80	131	1.2	437	2.4	49	1.1	6.1	222	7.5	2.3	0.26	310	112	2.9
Max	1186	4056	272	402	3.7	1286	8	110	3.3	29	1448	18	5.1	0.9	680	249	11
Min	16	1.4	1.5	15	0.51	1.9	0.76	0.18	1.2	7	605	0.33	0.15	0.46	0.05	0.95	0.43
42 Mean	23	6910	812	56	0.3	5061	37	39	3.2	4	96	39	3.1	1.3	344	198	41
S.D.	23	8283	896	54		4388	39	18	2.1	3	91	25	2.4	0.54	197	145	59
Max	70	20940	2184	148	0.54	10786	104	83	6.9	7	332	78	8.1	2.5	594	422	187
Min	17	472	18	11	0	142	0.93	21	1.4	0.33	11	12	0.95	0.68	93	16	0.11
43 Mean	75	625	116	44	1.9	366	0.49	9	0.75	5.3	439	3.1	1.5	0.40	31	87	10
S.D.	129	1118	212	57	3.2	912	0.36	9	0.76	4.8	252	2.2	1.5	0.24	38	76	11
Max	436	3675	658	165	11	2950	1.4	22	2.8	16	800	7.0	3.7	0.76	113	199	32
Min	13	4	1.0	6	0.39	2	0.68	0.14	0.90	0.05	0.89	0.48	0.13	0.25	0.04	0.43	0.11
49 Mean	8	0.15	0.79	542	6.0	0.90	0.37	3.4	2.4	13	663	0.25	0.09	0.25	0.02	0.83	5.3
S.D.		0.00		473	0.77		0.00	2.3	1.1	0.39	39	0.17	0.03	0.07		0.46	16
Max	15	0.30	1.6	1749	8	1.8	0.74	8.2	5.0	14	712	0.69	0.16	0.42	0.05	1.9	50
Min	0	0	0	206	5.3	0	0	0.48	1.4	13	588	0.32	0.15	0.40	0	0.29	0.12

Notes
Te: Only one sample showed any detectable concentrations: 42 mean 6.1, S.D. 8.4, max 23 and min 0.7 ppm.
Ba: Sample 41b showed data, mean 190, S.D. 399, max 1230 and min 4.7 ppm.
W: Sample 42 showed data, mean 0.33, S.D. 0.34, max 1.1 and min 0.18 ppm.

DISCUSSION

Classification of the Telfer Deposit

The style of mineralisation and genesis of the Telfer deposit is atypical and there are few readily identifiable analogues (Rowins *et al.* 1998). As a result, a variety of models have been applied to explain 'Telfer style' mineralisation. Earlier hypotheses included syngenetic exhalative (Tyrwhitt 1985), epigenetic replacement (Goellnicht *et al.* 1989), and the distal halo of a porphyry Cu-Au system (Dimo 1990). The currently accepted model takes into account the coincidence of several factors, considering the interrelationships between sedimentary environment, orogenesis and granite intrusions (Rowins *et al.* 1997).

The Paterson province is quite unlike most other Meso- to Neoproterozoic terrains in northern Australia. The dune-covered terrane appears to be a polymetallic mineral province of significant economic importance, if incompletely explored, with noteworthy uranium, base-metal and gold deposits already discovered (Groves *et al.* 1994). Forming as a result of syn- to post-collisional tectonic movement the province contrasts with the surrounding intra-cratonic basins (Goellnicht *et al.* 1989). Granitoids in the Paterson Province are also a unique age (~690 Ma) compared with other Proterozoic granites of northern Australia.

The Telfer mineralisation appears to have resulted from hot, saline, CO_2- and possibly also CH_4-bearing fluids (Goellnicht *et al.* 1989; Groves *et al.* 1994). Rowins *et al.* (1997) proposed that the granitoids may have contributed metals or sulphur to the

hydrothermal system, and may have driven large-scale thermal convection of heated saline waters sourced from the sedimentary rocks.

The present research has generated new petrographic and trace element data for pyrite and chalcopyrite in the context of ore textures. These data show the presence of a wide range of included minerals in pyrite and chalcopyrite, and a range of trace elements substituted within the sulphides which can give support for a modified model of ore genesis. Importantly, this modified model involves fluids and elements that may have been derived from a felsic intrusive source. Both the mineral inclusions and trace elements define a Sn-Ag-Bi geochemical signature with a distinct granitophile character.

At Telfer, the O'Callaghans granite is directly associated with complex gneiss and skarn zones, including magnetite skarns with a strong aeromagnetic expression. It is the only granite in the region known to be associated with extensive hydrothermal alteration systems and metal anomalies (W-Cu-Bi-Mo-Sn-Pb-Zn) (Newcrest 2014).

Although this study has not found direct evidence for W-and Mo-bearing minerals in the Telfer deposit, the Sn-Bi signature in the E-Reefs samples is striking. Fargher (2012) showed that the E-Reefs features a characteristic pyrite texture defined by the presence of <10 µm-sized, clustered multicomponent exsolution blebs of minerals containing (Bi-Sn-Cu ±Te, Au, Zn). The present study has confirmed the identities of these minerals and moreover, the presence of residual concentrations of the same elements in pyrite and chalcopyrite, their random orientation and typical cluster

formation, strongly suggests that the mineralized inclusions were released from pyrite during cooling. These granitic finger prints within the E-Reefs samples were not seen in comparative samples from the Middle Vale Reef, suggesting a later felsic hydrothermal event may have affected only the E-Reefs while the leaving the others 'untouched'.

Post-genetic Overprinting

The preservation of textures and distinct trace element distribution patterns are often important evidence for the multi-stage genetic development of an ore deposit (Arehart *et al.* 1993; Fleet *et al.* 1993; Oberthür *et al.* 1997; Genkin *et al.* 1998; Kouzmanov *et al.* 2002). At Telfer, Fargher (2012) showed that pyrite exhibit features that can only be explained as a result of multistage-ore genesis or the superposition of several distinct events. These include the presence of two or three textural and geochemical sub-types of pyrite within a single composite grain. Each was deposited from different hydrothermal fluids. The recognition, in the present study, of gersdorffite (Figure 4a) and arsenopyrite-bearing assemblages (Figure 5b) which are not seen in early-formed ores, are further evidence of such overprinting.

Furthermore, careful petrographic study has shown ample evidence for remobilisation and recrystallization of minerals within the deposit, as well as replacement of one mineral by another. Chalcopyrite, in particular, has been extensively remobilised and infills fractures in other minerals (Figures 3b and e, 4f, 5c and 6b, d and f). The common overprinting of chalcopyrite by bornite is another indicator of overprinting by this secondary event (Figures 3d-e), providing further evidence for the modification of the present genetic model of the Telfer deposit.

Towards A Broader Genetic Model

Groves (pers. comm. 2014) questioned established genetic models for Telfer and put forward the novel idea that the deposit is an analogue of Carlin-style gold systems typified by deposits of the Carlin Trend, Nevada, USA (Cline *et al.* 2005; Muntean *et al.* 2011). Carlin-style deposits are sediment-hosted deposits in which gold is microscopic and commonly present within the lattice of the host arsenian pyrite.

Rowins *et al.* (1998) suggested that the Telfer formation style required the coincidence of a number of geologic factors not dissimilar to the controls on the formation of a Carlin-style deposit (Muntean *et al.* 2011). Although Telfer and the Nevada deposits are clearly distinct in terms of geodynamic setting, age and host rocks, there are nevertheless some intriguing similarities at the larger scale. The Telfer deposit sits within a polymetallic province, and is surrounded by a range of differing deposit types, with varied ore types.

The Nifty deposit, located ~70 km west of Telfer displays similar pyrite textures to those at Telfer (Anderson *et al.* 2001). The euhdral pyrite, associated with hydrothermal alteration overprinting pyrite-bearing shale beds of the Nifty deposit corresponds to the Miles orogeny, much like the mineralisation at Telfer. The Nifty deposit was thought to have formed from fluids driven from deep in the Yeneena Basin (Anderson *et al.* 2001). Other surrounding deposits in the Paterson province include the Kintyre U-, Woodie Woodie Mn-, Magnum Au-Cu-Ag- and the O'Callaghans Cu, Zn and Pb skarn-deposits, as well as a number of Cu prospects. The Nevada Carlin-style deposits are also hosted within polymetallic provinces, although there is no similar trend between the certain

types of deposits surrounding deposits in the region; their ages also vary. Other deposit types present in Nevada include older SEDEX Au, barite, and base metals deposits; older pluton-related base and precious metal systems and younger hot spring Ag-Au and Hg deposits. Carlin-style mineralization has also been reported from China (Hu *et al.* 2002). Carlin gold-bearing terranes in China host older MVT-type base metals; older SEDEX barite systems and coeval Sb, As, Ti, Hg, U vein and replacement deposits. All deposit styles are hosted within calcareous marine sedimentary host rocks, at the edges of cratonic margins (Hu *et al.* 2002; Rowins *et al.* 1997). No consistent spatial or genetic relationships to coeval plutons are observed in any of these settings, although periodic episodes of hydrothermal activity produced thermal convection. Telfer-style mineralization sits within the domal structure, while the Carlin-style deposits sit within antiforms, stock work veins and along fault structures (Hofstra *et al.* 1999; Hu *et al.* 2002). The ages of the Telfer-, Nevada and Chinese Carlin-style deposits are different, ranging from the Neoproterozoic Telfer, to the Cretaceous Chinese systems, and mid-Tertiary Nevadan Carlin-style deposit.

A sedimentary source of ore metals has been suggested for all deposit styles. Like the Telfer deposits, the Nevada Carlin-style deposits were formed by flow of Au-bearing aqueous fluids into Fe-bearing carbonate rocks and subsequent sulphidation as the mechanism causing deposition of gold (Muntean *et al.* 2011). In both cases, there have been debate with respect to the contribution of magmatic or metamorphic fluids which would account for the geochemical signature of the mineralisation. It seems, modelling by Rowins *et al.* (1998) showed that the Telfer deposit requires a host rock with an average background gold concentration of no more than ~2-7 ppb for hydrothermal

activity to leach and transport the metals and deposit them in chemical- and structural-traps to form ore body. The Chinese Carlin-style deposits are found to be smaller and hosted in more siliceous rocks, whereas the Nevada deposits are larger and are hosted in more calcareous rocks (Hu *et al.* 2002).

The above discussion shows that there is no single model to account for the features of this disparate and intensely debated style of deposits. Comparison of Telfer with the Chinese and Nevada Carlin-style deposits highlights a number of similarities and represents an intriguing perspective. In all three cases, a combination of high paleo-thermal gradients and tectonic disturbance is indicated (Tu 1990; Hofstra *et al.* 1999; Hu *et al.* 2002). These requirements seem to have played an important role in the formation of the Telfer-stye and Carlin-style deposits.

Implications

Further data for, and interpretation of the trace element chemistry of sulphides within Telfer-style deposits will shed more light on the formation of the deposit and in turn, other known and yet to be discovered systems in the Paterson Province. Similarities between geological settings and the formations of deposit ore styles, such as Telfer- and Carlin-style deposits will guide development of invaluable exploration tools for additional deposits of comparable types in complex, multi-stage terranes.

A more detailed knowledge of the ore mineralogy and deportment of trace elements in the main sulphides will potentially facilitate more efficient processing of ore. Establishing the size and association of gold is also critical for maintaining gold recovery. The distribution of gold and other elements in mineral deposits will not, necessarily be consistent over all parts of the ore. The recognition of distinct

geochemical signatures in the E-Reefs samples is thus a valuable contribution to overall characterisation of the deposit.

This study has also contributed to fundamental information on the trace element chemistry of chalcopyrite. In the E-Reefs samples from Telfer, chalcopyrite is seen to host a broad range of trace elements, often at significant concentrations, higher than in many other ore systems. Provided that physical-chemical conditions of ore formation can be better constrained than they are at present, the trace element data will contribute to ongoing work to address whether there are systematic and predictable geochemical 'fingerprints' in chalcopyrite from different ore types that can serve as a basis for discriminating metal sources and fluid evolution.

CONCLUSIONS

This study has identified that the E-Reefs of the West Dome of the Telfer deposit shows very distinct trace element signatures when compared to the other reefs within the Telfer system. The characteristic textures of pyrite and chalcopyrite within the E-Reefs defines a marked Sn-Ag-Bi geochemical signature with a distinct granitophile character. Mineral inclusions and trace elements in the pyrite and chalcopyrite support a modified model of ore genesis for Telfer, expressing that a post formational event, involving a high temperature; hydrothermal episode, from felsic intrusive source has overprinted the E-Reefs.

The data set offers support for the hypothesis of Rowins *et al.* (1997) that the granitoids may have contributed metals or sulphur to the hydrothermal system, and may have

driven large-scale thermal convection of heated saline waters sourced from the sedimentary rocks.

Overprinting of the system shown through the preservation of textures and distinct trace element distribution patterns can only be explained as a result of multistage-ore genesis or the superposition of several distinct events.

ACKNOWLEDGMENTS

Firstly, thankyou to the staff from Adelaide Microscopy Angus Netting, Ben Wade, Ken Neubauer and Aoife McFadden for your training and patience.
The helpful suggestions and input from Ros King, Katie Howard and Bryony Crowe.
David Groves, I am very appreciative of the time you took to discuss and inspire; and Mathew Fargher for your helpful discussions and motivation.

Lastly, thank you to Nigel Cook for his generous support, guidance and direction throughout the year.

REFERENCES

ANDERSON B. R., GEMMELL J. B. & BERRY R. F. 2001. The Geology of the Nifty Copper Deposit, Throssell Group, Western Australia: Implications for Ore Genesis. *Economic Geology* **96** (7), 1535-1565

AREHART G.B., CHYSSOLIS S. L. & KESLER S. E. 1993. Gold and arsenic in iron sulphides from sediment-hsted disseminated gold deposits – implications for depositional processes. *Economic Geology and the Bulletin of the Society of Economic Geologists* **88**, 171-185.

BAGAS L. 2004a. The Neoproterozoic Throssel Range and Lamil Groups, northwest Paterson Orogen, Western Australia - a field guide: Western Australia. **Record 2004/15**. Geological Survey of Western Australia.

BAGAS L. 2004b. Proterozoic evolution and tectonic setting of the northwest Paterson Orogen, Western Australia. *Precambrian Research* **128**, 475-496.

CABRI L. J., CAMPBELL J. L., GILIES LAFLAMME J.H., LEIGH R.G., MAXWELL J.A. & SCOTT J.D. 1985. Proton-microprobe analysis of trace elements in sulfides from some massive-sulfide deposits. *The Canadian Mineralogist* **23**, 133-148.

CLARKE G.L. 1991. Proterozoic tectonic reworking in the Rundall Complex, Western Australia. *Australian Journal of Earth Sciences* **38**, 31-44.

CLINE J. S., HOFSTRA A. H., MUNTEAN J. L., TOSDAL R. M. & HICKEY K. A. 2005. Carlin-Type Gold Deposits in Nevada: Critical Geologic Characteristics and Viable Models. *Economic Geology 100th Anniversary Volume* , 451–484.

COOK N. J. & CHRYSSOULIS S. L. 1990. Concentrations of invisible gold in the common sulfides. *Canadian Mineralogist* **28**, 1-16.

COOK N. J., CIOBANU C. L. & PRING A. 2009. Trace and minor elements in sphalerite: A LA-ICP-MS study. *Geochimica et Cosmochimica Acta*, **73**, 4761-4791.

COOK N.J., CIOBANU C.L., GILES D. and WADE B. 2013. Correlating textures and trace elements in ore minerals. Mineral deposit research for a high-tech world. 12th Biennial SGA Meeting, 288-291.

CROWE B. 2014. The distribution of trace element chemistry in chalcopyrite. Honours thesis, University of Adelaide (unpubl).

DIMO G., 1990. Telfer gold deposits. In: Hughes, F.E. (Ed.), Geology of the Mineral Deposits of Australia and Papua New Guinea. *Australasian Institute of Mining and Metallurgy Monograph* **14**, 643-651.

DUROCHER K. E., KYSER T. K., MARLATT J. & HANLY A. 2003. New Ar-40/Ar-39 ages from the central Paterson Orogen, Western Australia. *Australian Journal of Earth Sciences* **50**, 601-610.

FARGHER M.R.K. 2012. Textural and LA-ICP-MS trace element chemistry analysis of pyrite from Telfer Au-Cu deposit, WA. Honours Thesis, University of Adelaide. (unpubl).

FLEET M. E., CHRYSSOULIS S. L., MACLEAN P. J., DAVIDSON R. & WEISENER C. G. 1993. Arsenian pyrtie from gold deposits - Au and As distribution investigated by SIMS and EMP, and color staining and surfice oxidation by XPS and LIMS. *Canadian Mineralogist* **31**, 1-17.

FYER B. J., JACKSON S. E. & LONGERICH H. P. 1995. Design, operation and role of the laser-ablation microbe coupled with an inductively coupled plasma-mass spectrometer (LA-ICP-MS) in the earth sciences. *Canadian Mineralogist* **33**, 303-312.

GENKIN A. D., BORTNIKOV N. S., CABRI L. J., WAGNER F. E., STANLEY C. J., SAFONOV G., MCMAHON G., FREIDL J., KERZIN A.L. & GAMYANIN G. N. 1998. A multidisciplinary study of invisible gold in arsenopyrite from four mesothermal gold deposits in Siberia, Russian Federation. *Economic Geology and the Bulletin of the Society of Economic Geologists* **93**, 463-478.

GEOLOGICAL SURVEY OF WESTERN AUSTRALIA. 1996. *Connaughton [cartographic material] / Geological Survey of Western Australia*. Geological Survey of Western Australia, East Perth, W.A.

GEORGE L., COOK N. J., CIOBANU C. L. 2014. Trace and minor elements in galena: A reconnaissance LA-ICP-MS study, Centre for Tectonics, Resources and Exploration (TRaX), University of Adelaide: [Dissertation].

GOELLNICHT N. M., GROVES D. I., MCNAUGHTON N. J. & DIMO G. 1989. an epigenetic origin for the Telfer gold deposit, Western Australia. *Economic Geology* **6**, 151 - 167.

GREY K., HOCKING R. M., STEVENS M. K., BAGAS L., CARLSEN G. M., IRIMIES F., PIRAJNO F., HAINES P. W. & APAK S. N. 2005. Lithostratigraphic nomenclature of the Officer Basin and correlative parts of the Paterson Orogen. . Geological Survey of Western Australia **89**.

GROVES D. I., BARLEY M. E. & SHEPHERD J. M. 1994. Geology and mineralization of Western Australia. *University of Western Australia Geology Department Extension Publication* **29**, 3-28.

GROVES D. I., GOLDFARB R. J., ROBERT F. & HART C.J.R. 2003. Gold deposits in metamorphic belts: overview of current understanding, outstanding problems, future research and exploration significance. *Economic Geology* **98**, 1-29.

HARRIS D. C., CABRI L. J., & NOBILING R. 1984. Silver bearing chalcopyrite, a principal source of silver in the Izok lake massive-sulfide deposit: confirmation by electron and proton-microprobe analyses. *The Canadian Mineralogist* **22**, 493-498.

HARRIS D. C. 1990. The Mineralogy of gold and its relevance to gold recoveries. *Mineralium Deposita* **25**, S3-S7.

HOFSTRA A. H., SNEE L. W., RYE R. O., FOLGER H. W., PHINISEY J. D., LORANGER R. J., DAHL A. R., NAESER C. W., STEIN H. J. & LEWCHUK M. 1999. Age constraints on Jerritt Canyon and other Carlin-type gold deposits in the western United States – relation to mid-Tertiary extension and magmatism. *Economic Geology* **94**, 769-802.

HU R-Z., SU W-C., BI X-W., TU G-Z. & HOFSTRA A. H. 2002. Geology and geochemistry of Carlin-type gold deposits in China. *Mineralium Deposita* **37**, 378-392.

HUSTON D. L., SIE S. H., SUTER G. F., COOKE D. R. & BOTH R. A. 1995. Trace elements in sulfide minerals from eastern Australian volcanic-hosted massive sulfide deposits; Part I, Proton microprobe analyses of pyrite, chalcopyrite, and sphalerite, and Part II, Selenium levels in pyrite; comparison with delta 34 S values and implications for the source of sulfur in volcanogenic hydrothermal systems. *Economic Geology* **90**, 1167-1196.

KOUZMANOV K., BAILLY L., RAMBOZ C., ROUCER O. & BÉNY J-M. 2002. Morphology, orogin and infrared microthermometry of fluid inclusions in pyrite from the Radka epithermal copper deposit, Srednogorie zone, Bulgaria. Mineralium Deposita **37**, 599-613.

LANGSFORD N. 2000. Geology and mineralisation of the Telfer district. *Newcrest Mining Limited*. (Unpubl).

LARGE R. R., MASLENNIKON V. V., ROBERT F., DANYUSHEVSKY L. V. & CHANG Z. 2007. Multistage sedimentary and metamorphic origin of pyrite and gold in the giant Sukhoi Log deposit, Lena gold province, Russia. *Economic Geology* **102**, 1233-1267.

LARGE R. R., DANYUSHEVSKY L., HOLLIT C., MASLENNIKOV V., MEFFRE S., GILBERT S., BULL S., SCOTT R., EMSBO P., THOMAS H., SINGH B. & FOSTER J. 2009. Gold and Trace Element Zonation in Pyrite Using a Laser Imaging Technique: Implications for the Timing of Gold in Orogenic and Carlin-Style Sediment-Hosted Deposits. *Economic Geology* **104**, 635-668.

MAXLOW J. & WILSON A. 2005. Paterson Province review and exploration strategy. *Newcrest Mining Limited*. (unpubl.).

MAXLOW J. 2007. Telfer geology. *Newcrest Mining Limited*. (unpubl.).

MOGGI-CECCHI V., CIPRIANI C., ROSSI P., CECCATO D., RUDELLO V. & SOMACAL H. 2002. Trace element contents and distribution maps of chalcopyrite: a micro-PIXE study. *Periodico di Mineralogia*, **71,**101-109.

MUNTEAN J. L., CLINE J. S., SIMON A. C. & LONGO A. A. 2011, Magmatic-hydrothermal origin of Nevada's Carlin-type gold deposits. *Nature Geoscience* **4,** 122-127.

NEWCREST MINING LIMITED. 2014. Annual Report. (unpubl.)

OBERTHUR T., WEISER T., AMANOR J. A. & CHRYSSOULIS S. L. 1997. Mineralogical siting and distribution of gold in quartz veins and sulfide ores of the Ashanti mine and other deposits in the Ashanti belt of Ghana: Genetic implications. *Mineralium Deposita* **32**, 2-15.

PIRAJNO F. & BAGAS L. 2008. A review of Australia's Proterozoic mineral systems and genetic models. *Precambrian Research* **166**, 54-80.

ROWINS S. M., GROVES D. I., MCNAUGHTON N. J., PALMER M. R. & ELDRIDGE C. S. 1997. A reinterpretation of the role of granitoids in the genesis of neoproterozoic gold mineralisation in the Telfer dome, western Australia. *Economic Geology and the Bulletin of the Society of Economic Geologists* **92**, 133-160.

ROWINS, S.M., GROVES, D.I. & MCNAUGHTON N..J. 1998. Neoproterozoic Telfer-style Au (Cu) deposits. *ASGO Journal of Australian Geology & Geophysics* **17**, 217-223.

SUNG Y. H., BRUGGER J., CIOBANU C. L., PRING A., SKINNER W. & NUGUS M. 2009. Invisible gold in arsenian pyrite and arsenopyrite from a multistage Archaean gold deposit: Sunrise Dam, Eastern Goldfields Province, Western Australia. *Miner Depos* **44**, 765-791.

TASESKA M., MAKRESKI P., STIBILJ V., JAĆIMOVIĆ R., STAFILOV T. & JOVANOVSKI G. 2008. Determination of trace elements in chalcopyrite (CuFeS2) by k0-instrumental neutron activation

analysis after matrix elements removal. *Macedonian Journal of Chemistry and Chemical Engineering* **27**, 141-147.

THOMAS H. V., LARGE R. E., BULL S. W., MASLENNIKOV V., BERRY R. F., FRAZER R., FROUD F. & MOYE R. 2011. Pyrite and pyrrhotite textures and composition in sediments, laminated quartz veins, and reefs at Bendigo Gold Mine, Australia: insights for ore genesis. *Economic Geology* **106**, 1-31.

TU G. 1990. The SW Qinling and the SW Guizhou uranium and gold metallogenic belts, and their similarities to the Carlin-type gold deposits in the western states, USA. *Uranium Geology* **6**, 321–325

TYRWHITT D. S. 1985. Exploration, development, and geology of the Telfer gold mine, Great Sandy Desert, Western Australia. *Prosepecting in Arid Areas International Conference,* Rabat, Morocco,11- 19. Institute of Mining and Metallurgy, London, UK.

WILLIAMS I. R. & MYERS J. S. 1990. *Paterson Orogen, in Geology and mineral resources of Western Australia*. Survey. W. A. G. 282 - 283.

WINDERBAUM L., CIOBANU C. L., COOK N. J., PAUL M., METCALFE A. & GILBERT S. 2012. Multivariate Analysis of an LA-ICP-MS Trace Element Dataset for Pyrite. *Mathematical Geosciences* **44**, 823-842.

APPENDIX A: METHODOLOGY

Analytical Approach

Using a combination of techniques such as scanning electron microscopy (SEM), electron probe micro-analysis (EPMA) and laser ablation inductively-coupled plasma mass spectrometry (LA-ICP-MS) allows the extraction of information on both the spatial and chemical distributions of elements within minerals (e.g. Fryer *et al.* 1995). This permits better evaluation of significance of trace element concentrations, especially for those for which an extremely low limit of detection is required (Fryer *et al.* 1995). Scanning electron microscopy (SEM) was conducted on samples to give a clear identification of the minerals of interest and their relationships. Through the use of back-scatter electron (BSE) imaging, information about the mineral textures, intergrowths and compositional zoning can be observed and visually captured. The characterization of these mineral inclusions within the major minerals was important for the selection of areas for trace element analysis.
An electron probe micro-analyser (EPMA) was used to obtain quantitative major and minor element compositional data for minerals whose composition can vary, providing additional petrogenetic information about the samples.
Finally, LA-ICP-MS was used to determine quantitative trace element concentrations in specific minerals. Precise determination trace element concentrations have been inaccessible until recent times, as a result of the high minimum detection limits associated with EPMA (Cook *et al.* 2013). With the use of the LA-ICP-MS, used in conjunction with SEM and EPMA, the detection limits are able to detect samples from as low as 0.05 ppm for some elements, allowing the rapid *in-situ* chemical analysis of individual minerals within mineral samples (Watling *et al.* 1995). The larger sample volume used for LA-ICP-MS compared to EPMA does, however, enforce a trade-off with respect to the ability to analyse the smallest areas.

Sampling

Newcrest Mining Limited selected suitable drill core with significant representative intersections of pyrite and mineralisation from the West dome deposit (Figure 1c) Mineralised reef and syngenetic pyrite intersects were identified from assay results, Newcrest log cores and core photos were sampled. The aim was to have a sample suite spatially representative of the E-Reefs of the west dome. Diamond drill hole WRC28601 was used (Fargher 2012).

Samples for mineralogical and petrographic analysis were prepared as one-inch polished sections at Adelaide Petrographics.

Experimental Details

All microanalytical work was performed at Adelaide Microscopy (University of Adelaide).

SEM ANALYSIS

Each sample was examined by optical and scanning electron microscopy (SEM) confirms the identification of minerals within the samples and investigates their mutual relationships. The SEM work involved the use of a Quanta 450 instrument, equipped with a EDAX team energy dispersive X-ray spectroscopy (EDS) silicon drift detector (SDD) and back-scatter electron (BSE) detector, to produce digital images. This imaging was used to characterise mineral associations and to document significant textures and mineralogical relationships, and in particular, to visualise compositional zoning within individual mineral grains. EDAX allows semi-quantitative analysis of minerals to further analyse such mineral characteristics. Operation of the SEM involved back-scatter mode at an accelerated voltage of 20kv, with a spot size of approx. 1-2 microns.

LA-ICP-MS SPOT ANALYSIS

LA-ICP-MS was used on samples 41a, 41b, 41c, 41s, 42, 43 and 49 to provide quantitative trace element concentration data for calc-silicate and accessory minerals. A Resonetics M-50-LR 193-nm Excimer laser microprobe coupled to an Agilent HP-7700cx Quadrupole ICP-MS was used for analysis. This instrument provides minimum limits of detection as low as 0.05ppm range for some elements. Particular attention was paid to the concentrations of REE and other trace elements of petrogenetic value. Glitter software was used for data reduction (Van Achterbergh *et al.* 2001). The table below shows the settings used for the mircoanalysis.

Parameters	Value
Spot size (µm)	30
Pulse rate (Hz)	5
Power level (%)	85
Laser energy (J/cm^{-2})	6-9
Ablation rate (µm/s^{-1})	~1.5

Through this analysis the following isotope suite was monitored: ^{23}Na, ^{29}Si, ^{33}S, ^{34}S, ^{43}Ca ^{51}V ^{53}Cr, ^{55}Mn, ^{57}Fe, ^{59}Co, ^{60}Ni, ^{65}Cu, ^{66}Zn, ^{69}Ga, ^{75}As, ^{82}Se, ^{95}Mo, ^{107}Ag, ^{111}Cd, ^{115}In, ^{118}Sn, ^{121}Sb, ^{125}Te, ^{137}Ba, ^{182}W, ^{193}Ir, ^{197}Au, ^{202}Hg, ^{205}Ti, ^{206}Pb, ^{207}Pb, ^{208}Pb, and ^{209}Bi. Measuring multiple isotopes of Fe, Ti and Pb tested the consistency of the data. Each spot was analysed for a total of 118 s, in which time the background was measured for 30 s (laser off) and the unknown was measured for the remaining 88 s (laser on).
Standard reference materials were NIST-612 using coefficients given by Pearce *et al.* (1997) and the sulphide reference material Mass 1 sulphide pressed pellet standard (Wilson *et al.* 2002). Standards were run after each 10-20 unknowns; detection limits were calculated for each element in each spot analysis. Data reduction was undertaken using Fe as the internal standard for pyrite.

References

COOK N. J., CIOBANU C. L., GILES D. & WADE B. 2013. Correlating textures and trace elements in ore minerals. In: Mineral deposit research for a high-tech world. 12th Biennial SGA Meeting, 12-15 August 2013, Uppsala, Sweden. 288-291.

FRYER B. J., JACKSON S. E. & LONGERICH H. P. 1995. Design, operation and role of the laser-ablation microbe coupled with an inductively coupled plasma-mass spectrometer (LA-ICP-MS) in the earth sciences. Canadian Mineralogist **33**, 303-312.

PEARCE N., PERKINS W.T., WESTGATE J.A., GORTON M.P., JACKSON S.E., NEAL C.R. & CHENERY S.P. 1997. A compilation of new and published major and trace element data for NIST SRM 610 and NIST SRM 612 glass reference material. Geostandards Newsletter **21,** 115–144.

VAN ACHTERBERGH E., RYAN C.G., JACKSON S.E. & GRIFFIN W.L., 2001. LA-ICP-MS in the Earth Sciences - Appendix 3, data reduction software for LA-ICP-MS. In: Sylvester, P.J. (Ed.), Mineralogical Association of Canada Short Course, **29**, 239-243.

WATLING R.J., HERBERT H.K. & ABELL I.D. 1995. The application of laser ablation-inductively coupled plasma-mass spectrometry (LA-ICP-MS) to the analysis of selected sulfide minerals. Chemical Geology **124**, 67-81.

WILSON S. A., RIDLEY W. I. & KOENIG A. E., 2002. Development of sulphide calibration standards for the laser ablation inductively-coupled plasma mass spectrometry technique. United States Geological Survey.